This is the accepted version of an article published in 2018 IEEE International Conference on Environment and Electrical Engineering and 2018 IEEE Industrial and Commercial Power Systems Europe - EEEIC/I&CPS Europe
DOI: 10.1109/EEEIC.2018.8493932

Effect of Including Transient Virtual Impedance in Droop-Controlled Microgrids

Fredrik Göthner, Ole-Morten Midtgård
Norwegian university of Science and Technology
Trondheim, Norway

Raymundo Torres-Olguin, Salvatore D'Arco
SINTEF Energy
Trondheim, Norway

***Abstract*—Droop control has shown promising results for decentralized power sharing in microgrids. However, the basic scheme can suffer from unequal reactive power sharing power due to differing line impedances between converters and due to the predominantly resistive nature of low voltage networks. Virtual impedances are able to mitigate these drawbacks, and are mostly implemented using a quasi-stationary approach. This approach replicates an impedance in steady state, but transients of the load current are only partly reproduced. This paper discusses the effect of including the transient term of the virtual impedance. A state-space small-signal model is derived in order to show the effect of including the transient virtual impedance. Simulations of a two-inverter microgrid are also shown to test the model and offer a numerical example. Both modal analysis on the small-signal model and the results from the simulation indicate improved damping when including the transient virtual impedance.**

I. Introduction

The increasing share of microsources in the grid have paved the way for microgrids, being able to operate both grid connected and islanded. The advantages of microgrids include improved reliabilty, reduced feeder losses and the possibility for delivering ancillary services [1], [2]. One of the main challenges of islanded operation with a large penetration of power electronics interfaced distributed generation (DG) units is the lack of rotating inertia, which can lead to large deviations in frequency unless a proper control mechanism is implemented [3].

A well-known strategy for solving this issue is based on the droop method [4], in order to ensure that the system frequency and voltage deviations are within acceptable limits. One of the drawbacks of the conventional droop method, however, is its inability of ensuring proper reactive power sharing in the presence of a mismatch between the line impedances of different inverters [5]. Moreover, the conventional droop is not able to decouple the control of active and reactive power in dominantly resistive grids [6].

The issues of active and reactive power coupling and reactive power sharing can be solved by applying virtual impedances. A review of how these can be implemented in voltage source converters (VSCs) is given in [7]. In particular, virtual impedances modifying the outer voltage loop are found to be able to improve reactive power sharing and reduce active and reactive power coupling.

In [5], a virtual inductance is utilized to obtain improved decoupling and a proper power balance for a single phase system, while a virtual resistance is employed in [8] due to application of opposite droop. For three-phase systems, the most common implementations are based on the stationary reference frame. An example of that is given in [9], which presents a design and implementation approach for virtual impedances. Another example is given in [10], in which a virtual negative resistor is utilized in order to improve power sharing.

A small-signal model of a single inverter employing droop control is given in [11]. In particular, the paper deals with the current, voltage and droop control, in addition to the plant model. In [12], transfer functions are used to model a single inverter where also virtual impedances are implemented. Here, the transient term of the virtual impedance is included in the theoretical study, but the difference to modelling the virtual impedance with a quasi-stationary approach is not shown. The aim of this paper is, therefore, to investigate the effect that the transient virtual impedance can have on the stability and regulation of the system.

The outline of the paper is as follows. Section II describes the implementation of an outer virtual impedance for both the stationary and the synchronous reference frame. Section III describes the modelling of a single inverter using a droop controller with virtual impedances, in addition to inner voltage and current control. Section IV establishes the linearized small-signal model and discusses the effect that the transient part of the virtual impedance has on the performance. Finally, Section V shows the results of a simulation example in order to investigate the linearized model, before Section VI concludes the paper.

II. Virtual Impedance Implementation

This section will explain the implementation of virtual impedances in the stationary and in the synchronous reference frames.

A. Virtual Impedance in the Stationary Reference Frame

The voltage drop across an inductive-resistive line in the stationary reference frame is given by (1) and (2):

$$\Delta V_\alpha = R_l i_\alpha + L_l \frac{di_\alpha}{dt} \tag{1}$$

978-1-5386-5186-5/18/$31.00 © 2018 IEEE

This is the accepted version of an article published in 2018 IEEE International Conference on Environment and Electrical Engineering and 2018 IEEE Industrial and Commercial Power Systems Europe - EEEIC/I&CPS Europe
DOI: 10.1109/EEEIC.2018.8493932

$$\Delta V_\beta = R_l i_\beta + L_l \frac{di_\beta}{dt} \tag{2}$$

where L_l and R_l are the inductance and resistance of the line, $\Delta V_{\alpha\beta}$ are the voltage drops of the line and $i_{\alpha\beta}$ are the line currents, in the α and β axes, respectively.

An outer virtual impedance can, thus, be implemented by subtracting (1) and (2) from the desired voltage reference [7]. However, in order to avoid amplification of high frequency noise, the term containing the derivative of the current needs to be modified [7]. A first option is to apply a quasi-stationary approach [9], as given in (3) and (4)

$$\Delta V_\alpha = R_l i_\alpha - \omega L_l i_\beta \tag{3}$$

$$\Delta V_\beta = R_l i_\beta + \omega L_l i_\alpha \tag{4}$$

where ω is the system frequency. This virtual impedance replicates the response of an actual impedance at steady state. The difference from a real impedance is that it does not include the derivative term, and hence present different transient behaviour. A second option is to apply a low-pass filter (LPF) to the derivative term, in order to limit its high-frequency effects. While this approach can model the transient response of the virtual impedance to resemble an actual impedance more closely, it also affects the phase of the signal in steady state [7].

B. Virtual Impedance in the Synchronous Reference Frame

The voltage drop in the synchronous reference frame over an inductive-resistive feeder is given by

$$\Delta V_d = R_l i_d - \omega L_l i_q + L_l \frac{di_d}{dt} \tag{5}$$

$$\Delta V_q = R_l i_q + \omega L_l i_d + L_l \frac{di_q}{dt} \tag{6}$$

Thus, a virtual impedance can be implemented by subtracting (5) and (6) from the desired voltage reference. Just as for the implementation in the stationary reference frame, the high-frequency effects of the derivative action must be limited. Here, the quasi-stationary approach can be implemented by neglecting the derivative term altogether, as the cross-coupling effects are present in the steady-state response. Another option is to apply an LPF to the derivative term, as in

$$\Delta V_d = R_l i_d - \omega L_l i_q + \eta_d \tag{7}$$

$$\Delta V_q = R_l i_q + \omega L_l i_d + \eta_q \tag{8}$$

where n_{dq} are the low-pass filtered transient terms given by

$$\eta_d = \frac{\omega_{c2}}{s + \omega_{c2}} s L_l i_d \tag{9}$$

$$\eta_q = \frac{\omega_{c2}}{s + \omega_{c2}} s L_l i_q \tag{10}$$

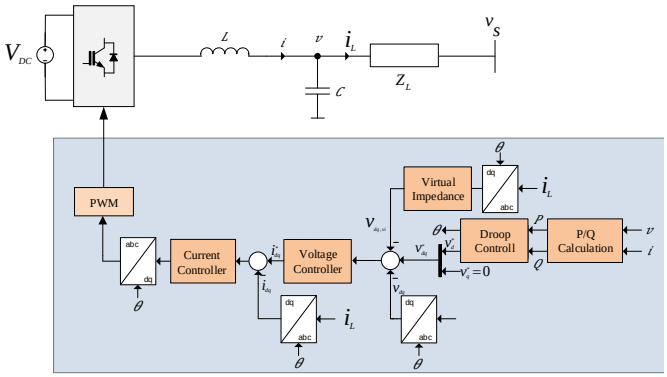

Fig. 1: Droop control scheme including virtual impedance

where w_{c2} is the cutoff frequency of the LPF. Thus, for implementing virtual impedances using a quasi-stationary approach, (9) and (10) can be used with $\eta_{dq} = 0$.

Contrary to the virtual impedance in the stationary reference frame, this approach only alters the phase during transients, while not affecting the steady state. Hence, there could be an advantage of using the virtual impedance in the synchronous reference frame over that of the stationary reference frame, since the transient dynamic term can be included in the response. This is possible due to the variables being constant in the synchronous reference frame.

Having a large value for the virtual inductance, an inductive output impedance as seen from the inverter can be obtained, leading to reduced coupling of active and reactive power in the conventional droop control [5]. Moreover, if the virtual impedance is sufficiently large, this can partly compensate for mismatch in the feeder impedances, thus leading to improved reactive power sharing. On the other hand, a too large virtual impedance will also limit the output voltage of the inverter, and, hence, also the power that can be delivered. Thus, a trade-off exists between improved power sharing and the magnitude of the delivered power.

III. Modelling of a Single Inverter

This section provides the detailed description of the modelling of a single inverter. The control of the inverter with its accompanying LC-filter is seen in Fig. 1. The dc side dynamics is neglected by assuming a constant dc voltage source. Moreover, by neglecting the switching behaviour, an average model for the converter is assumed [11]. The control of the inverter is performed in the synchronous reference frame and is based on that of grid-supporting VSCs [2]. The control consists of an inner current control, and outer voltage control. The reference for the voltage controller comes from the difference between the droop controller and the virtual impedance calculation. The droop controller in turn gets its input from the low-pass filtered power calculation of the inverter output power. For islanded operation, it suffices to integrate the droop frequency and use this angle as a reference for the Park transformations [2]. In the following, each of the

This is the accepted version of an article published in 2018 IEEE International Conference on Environment and Electrical Engineering and 2018 IEEE Industrial and Commercial Power Systems Europe - EEEIC/I&CPS Europe
DOI: 10.1109/EEEIC.2018.8493932

sub-blocks of Fig. 1 will be presented, in addition to the plant to be controlled.

A. Droop Control

The droop controller ensures stable operation of the microgrid by adjusting the angular frequency and voltage setpoints, ω and E so as to ensure a proper sharing between different units. In particular, this is obtained by applying the conventional droop equations:

$$\omega = \omega^* - m(P - P^*) \tag{11}$$

$$E = E^* - n(Q - Q^*) \tag{12}$$

where ω^* is angular frequency reference, E^* is the droop control voltage reference, m and n are the droop gains, P^* and Q^* are the active and reactive power references, while P and Q are the measured active and reactive powers. The latter are obtained by low-pass filtering the instantaneous active and reactive powers [11], as given in:

$$P = \frac{\omega_{c1}}{s + \omega_{c1}}(v_d i_{Ld} + v_q i_{Lq}) \tag{13}$$

$$Q = \frac{\omega_{c1}}{s + \omega_{c1}}(v_d i_{qd} - v_q i_{Ld}) \tag{14}$$

where ω_{c1} is the cut-off frequency of the LPF, v_{dq} are the voltages at the filter capacitor and i_{Ldq} are the inverter output currents. Finally, the angle to be used for the dq-transformations is given by:

$$\theta = \int \omega dt \tag{15}$$

B. Voltage Controller

The voltage controller regulates the voltage at the filter capacitor. It consists of a PI controller and feedforward and decoupling terms, given by (16) and (17).

$$i_d^* = K_{pv}(v_d^* - v_d) + K_{iv}C_{Vd} - \omega C v_q + i_{Ld} \tag{16}$$

$$i_q^* = K_{pv}(v_q^* - v_q) + K_{iv}C_{Vq} + \omega C v_d + i_{Lq} \tag{17}$$

Here K_{pv} and K_{iv} are the proportional and integral gain of the PI controller, i_{dq}^* are the references for the current controller, and C_{Vd} and C_{Vd} are given by:

$$C_{Vd} = \int (v_d^* - v_d)dt \tag{18}$$

$$C_{Vq} = \int (v_q^* - v_q)dt \tag{19}$$

where v_{dq}^* are the voltage references. When including virtual impedances, the voltage references are given according to:

$$v_d^* = E + \omega L_{vi} i_{Lq} - R_{vi} i_{Ld} - \eta_d \tag{20}$$

$$v_q^* = -\omega L_{vi} i_{Ld} - R_{vi} i_{Lq} - \eta_q \tag{21}$$

where L_{vi} and R_{vi} are the virtual inductance and resistance.

C. Current Controller

Based on the current references in (16) and (17), the current controller regulates the inverter side filter current. This controller is also based on a PI controller, in addition to decoupling terms and feedforward of the capcitor voltage as seen in (22) and (23).

$$u_d^* = K_{pi}(i_d^* - i_d) + K_{ii}C_{Id} - \omega L i_q + v_d \tag{22}$$

$$u_q^* = K_{pi}(i_q^* - i_q) + K_{ii}C_{Iq} + \omega L i_d + v_q \tag{23}$$

Here, u_d^* and u_q^* are the reference voltages for the inverter voltage, C_{Id} and C_{Iq} are the states of the PI integrator, while K_{pi} and K_{ii} are the proportional and integral gains of the PI controller.

D. Plant Model

Finally, the first order plant is based on the filter inductor L with its resistance R, the filter capacitor C, and the equivalent line impedance consisting of the inductance L_L and the resistance R_L. Thus, the plant equations are given by:

$$L\frac{di_d}{dt} = u_d - v_d + \omega L i_q - R i_d \tag{24}$$

$$L\frac{di_q}{dt} = u_q - v_q - \omega L i_d - R i_q \tag{25}$$

$$C\frac{dv_d}{dt} = i_d - i_{Ld} + \omega C v_q \tag{26}$$

$$C\frac{dv_q}{dt} = i_q - i_{Lq} - \omega C v_d \tag{27}$$

$$L_L\frac{di_{Ld}}{dt} = v_d - v_{sd} + \omega L_L i_{Lq} - R_L i_{Ld} \tag{28}$$

$$L_L\frac{di_{Lq}}{dt} = v_q - v_{sq} - \omega L_L i_{Ld} - R_L i_{Lq} \tag{29}$$

where v_{sdq} is the load voltage.

IV. Effect of Including Transient Virtual Impedance

In order to analyze the effect the transient virtual impedance has on the stability and performance of the droop controlled microgrid, a small-signal model of a single inverter is derived by linearizing equations (12)-(29), and assuming $u_{dq}^* = u_{dq}$. The free motion of the system can be then given as

$$\Delta\dot{x} = A\Delta x \tag{30}$$

where Δx and A are given in (31) and (32). For the case without transient virtual impedance, the system matrix corresponds to the subset of the first 13 rows and columns of (32).

$$\Delta x = [\Delta\theta \quad \Delta P \quad \Delta Q \quad \Delta C_{Vdq} \quad \Delta C_{Idq} \quad \Delta i_{dq} \quad \Delta v_{dq} \quad \Delta i_{Ldq} \quad \Delta\eta_{dq}]^T \tag{31}$$

This is the accepted version of an article published in 2018 IEEE International Conference on Environment and Electrical Engineering and 2018 IEEE Industrial and Commercial Power Systems Europe - EEEIC/I&CPS Europe
DOI: 10.1109/EEEIC.2018.8493932

$$A = \begin{bmatrix}
0 & -m & 0 & 0 & 0 & 0 & 0 & 0 & 0 & 0 & 0 & 0 & 0 & 0 & 0 & 0 \\
0 & -\omega_{c1} & 0 & 0 & 0 & 0 & 0 & 0 & 0 & \omega_{c1}I_{Ld0} & \omega_{c1}I_{Lq0} & \omega_{c1}V_{d0} & \omega_{c1}V_{q0} & 0 & 0 \\
0 & 0 & -\omega_{c1} & 0 & 0 & 0 & 0 & 0 & 0 & \omega_{c1}I_{Lq0} & -\omega_{c1}I_{Ld0} & -\omega_{c1}V_{q0} & \omega_{c1}V_{d0} & 0 & 0 \\
0 & -mL_{vi}I_{Lq0} & -n & 0 & 0 & 0 & 0 & 0 & 0 & -1 & 0 & -R_{vi} & \omega_0 L_{vi} & -1 & 0 \\
0 & mL_{vi}I_{Ld0} & 0 & 0 & 0 & 0 & 0 & 0 & 0 & 0 & -1 & -\omega_0 L_{vi} & -R_{vi} & 0 & -1 \\
0 & -mL_{vi}I_{Lq0}K_{pv} & -nK_{pv} & K_{iv} & 0 & 0 & 0 & -1 & 0 & -K_{pv} & -\omega_0 C & 1-R_{vi}K_{pv} & K_{pv}\omega_0 L_{vi} & -K_{pv} & 0 \\
0 & mL_{vi}I_{Ld0}K_{pv} & 0 & K_{iv} & 0 & 0 & 0 & -1 & 0 & \omega_0 C & -K_{pv} & -K_{pv}\omega_0 L_{vi} & 1-R_{vi}K_{pv} & 0 & -K_{pv} \\
0 & -\frac{mL_{vi}I_{Lq0}}{L} - mI_{q0} & -\frac{nK_{pc}K_{pv}}{L} & \frac{K_{pc}K_{iv}}{L} & 0 & \frac{K_{pc}}{L} & 0 & -\frac{R+K_{pc}}{L} & 0 & -\frac{1+K_{pc}K_{pv}}{L} & -\frac{K_{pc}\omega_0 C}{L} & \frac{K_{pc}}{L}(1-K_{pv}R_{vi}) & \frac{K_{pc}K_{pc}\omega_0 L_{vi}}{L} & -\frac{K_{pc}K_{pc}}{L} & 0 \\
0 & \frac{mL_{vi}I_{Ld0}}{L} + mI_{d0} & 0 & \frac{K_{pc}K_{iv}}{L} & 0 & \frac{K_{pc}}{L} & 0 & -\frac{R+K_{pc}}{L} & 0 & \frac{K_{pc}\omega_0 C}{L} & -\frac{1+K_{pc}K_{pv}}{L} & -\frac{K_{pc}K_{pc}\omega_0 L_{vi}}{L} & \frac{K_{pc}}{L}(1-K_{pc}R_{vi}) & 0 & -\frac{K_{pc}K_{pc}}{L} \\
0 & -mV_{q0} & 0 & 0 & 0 & 0 & 0 & \frac{1}{C} & 0 & 0 & \omega_0 & -\frac{1}{C} & 0 & 0 & 0 \\
0 & mV_{d0} & 0 & 0 & 0 & 0 & 0 & \frac{1}{C} & 0 & -\omega_0 & 0 & 0 & -\frac{1}{C} & 0 & 0 \\
\frac{1}{L_L}(V_{sD}\sin\theta_0 - V_{sQ}\cos\theta_0) & -mL_{Lq0} & 0 & 0 & 0 & 0 & 0 & 0 & 0 & \frac{1}{L_L} & 0 & -\frac{R_L}{L_L} & \omega_0 & 0 & 0 \\
\frac{1}{L_L}(V_{sD}\cos\theta_0 + V_{sQ}\sin\theta_0) & mL_{Ld0}) & 0 & 0 & 0 & 0 & 0 & 0 & 0 & 0 & \frac{1}{L_L} & -\omega_0 & -\frac{R_L}{L_L} & 0 & 0 \\
\frac{2\omega_{c2}L_{vi}}{L_L}(V_{sD}\sin\theta_0 - V_{sQ}\cos\theta_0) & -\omega_{c2}L_{vi}mI_{Lq0} & 0 & 0 & 0 & 0 & 0 & 0 & 0 & \frac{w_{c2}L_{vi}}{L_L} & 0 & -\frac{\omega_{c2}L_{vi}R_L}{L_L} & \omega_{c2}L_{vi}\omega_0 & -\omega_{c2} & 0 \\
\frac{2\omega_{c2}L_{vi}}{L_L}(V_{sD}\cos\theta_0 + V_{sQ}\sin\theta_0) & \omega_{c2}L_{vi}mI_{Ld0} & 0 & 0 & 0 & 0 & 0 & 0 & 0 & 0 & \frac{w_{c2}L_{vi}}{L_L} & -\omega_{c2}L_{vi}\omega_0 & -\frac{\omega_{c2}L_{vi}R_L}{L_L} & 0 & -\omega_{c2}
\end{bmatrix} \tag{32}$$

TABLE I: Parameters for Test Set-Up

Parameter	Value	Parameter	Value
Line-line voltage	400 V	V_{d0}	329.6 V
Rated Power	3 kVA	V_{q0}	1.6 V
ω_0	$2\,\pi 50$	V_{sd}	326.6 V
L	500 µH	I_{d0}	6.1 A
R	0.01 Ω	I_{q0}	5.2 Ω
C	50 µF	I_{Ld0}	6.1 A
L_L	830 µH	I_{Lq0}	0
R_L	0.5 Ω	θ_0	0.28°
L_{vi}	600 µH	w_{c1}	31.4 rad/s
R_{vi}	0.05 Ω	w_{c2}	500 rad/s
m	2.1×10^{-4} Hz/W	K_{pc}, K_{ic}	2.63, 400
n	0.0011 V/VAr	K_{pv}, K_{iv}	0.05, 19.5

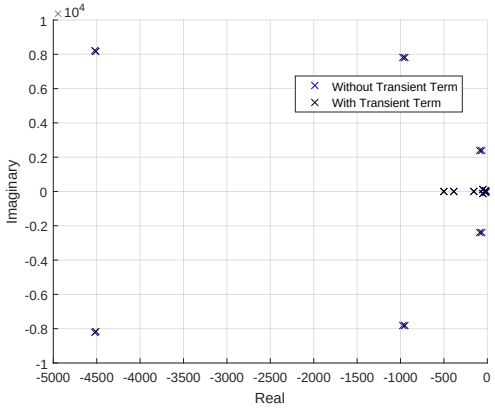

Fig. 2: Eigenvalues of the system with and without transient virtual impedance

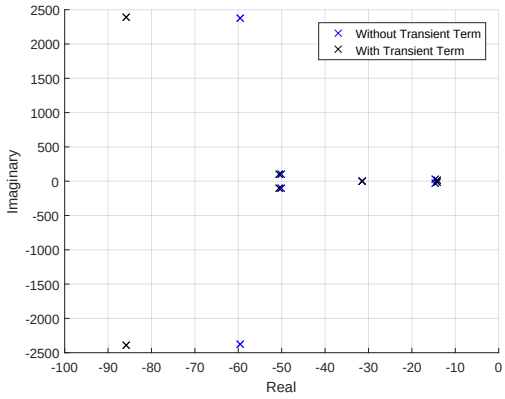

Fig. 3: Effect of adding transient virtual impedance on the low-frequency modes

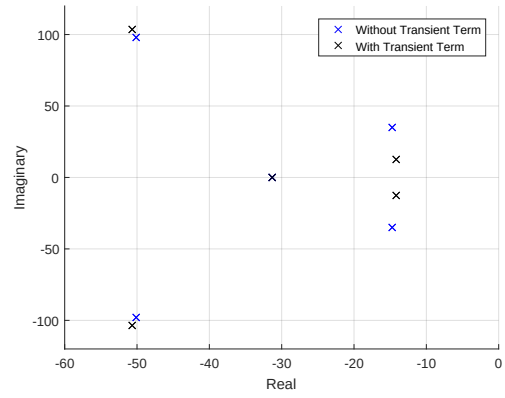

Fig. 4: Enlarged view of the effect of adding transient virtual impedance on the low-frequency modes

A. Modal Analysis

The modes of the systems with and without transient virtual impedance were found by solving $\det(\lambda I - A) = 0$, using the operating point and system parameters according to Table I. The resulting modes of both systems are shown in Fig. 2. It can be seen that there are three main clusters of modes, corresponding to the cascaded control loops of the controller. There are a total of 15 modes corresponding to the 15 states of the system for the description with transient virtual impedance, whereas there are 13 modes corresponding to the 13 states for the system using quasi-stationary virtual impedance.

Fig. 3 displays how the low-frequency modes differ when the transient virtual impedance is included. It can be seen that the damping of the most oscillatory modes is improved by moving their real part from about -60 to -86. An enlarged view of the same plot can be seen in Fig. 4. Here, it is evident that the transient virtual impedance barely changes the damping of the left-most poles, as both the imaginary and real part of the modes are increased slightly. The real pole around -31 is barely affected by the transient virtual impedance. The rightmost pair of eigenvalues clearly increases its damping, although achieving a slightly larger real value. Hence, for the example considered, including the transient virtual impedance improves the damping of the system.

The plot in Fig. 5 displays the sensitivity of the system with

This is the accepted version of an article published in 2018 IEEE International Conference on Environment and Electrical Engineering and 2018 IEEE Industrial and Commercial Power Systems Europe - EEEIC/I&CPS Europe
DOI: 10.1109/EEEIC.2018.8493932

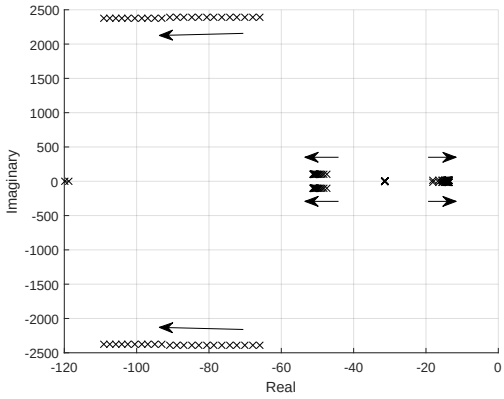

Fig. 5: Trace of low-frequency modes as a function of low-pass filtering of the transient virtual impedance: $100 \leq w_{c2} \leq 1000$

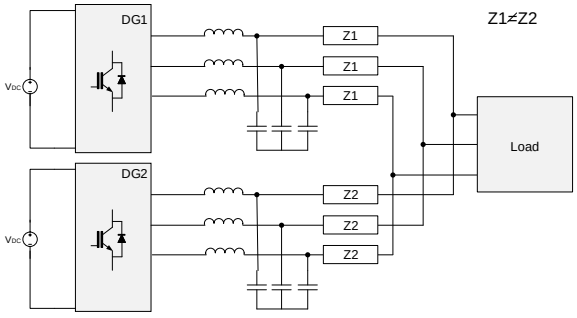

Fig. 6: Microgrid system consisting of two inverters supplying a parallel load.

transient virtual impedance to the cut-off frequency of the low-pass filter. As seen in the figure, the two leftmost conjugated modes achieve improved damping when the cut-off frequency is increased. Meanwhile, the modes closest to the imaginary axis move toward the unstable region, and achieve reduced damping. Hence, there is a trade-off in choosing the cut-off frequency of the transient virtual impedance.

V. Numerical Simulation

In order to test the model with regards to including the transient virtual impedance, the microgrid in Fig. 6 was simulated. The microgrid is operated in island mode, where two DG units are supplying a common linear, balanced load. The parameters for the test configuration are given in Tables I and II. In particular, the value of the line impedance was 25 % larger for DG2, while the X/R ratio was 0.5.

TABLE II: Simulation Parameters

Parameter	Value
V_{dc}	800 V
f_{sw}	8 kHz
Z_1	$0.5 + j0.25\ \Omega$
Z_2	$0.625 + j0.313\ \Omega$

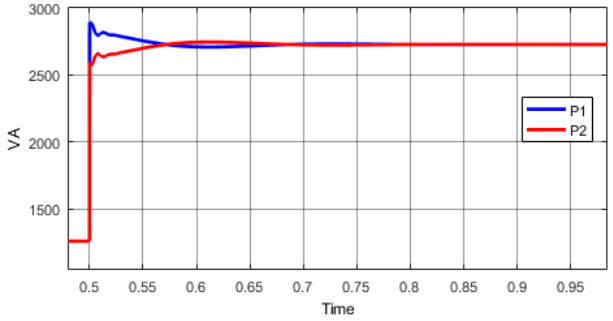

Fig. 7: Active power of inverters without transient virtual impedance

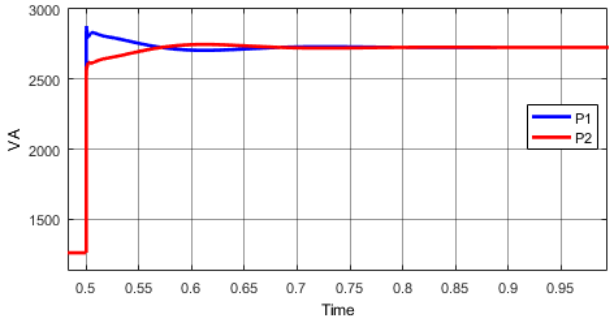

Fig. 8: Active power of inverters with transient virtual impedance

Fig. 7 shows the active power supplied by each inverter when the transient virtual impedance is disabled. At $t = 0.5\,\mathrm{s}$, the load is stepped from $2.5\,\mathrm{kW}$ to $5.5\,\mathrm{kW}$. From the figure, it is evident that the sharing mechanism works well, but there is an initial oscillation in the sharing of the power.

Fig. 8 displays the active power supplied by each inverter when the transient portion of the virtual impedance is included. The sharing between the two inverters is still good, and in steady state it is identical to the case without transient virtual impedance. However, immediately following the step in the load, there is less oscillation of the power compared to the case without the transient term of the virtual impedance.

VI. Conclusion

This paper has presented some fundamental considerations when applying virtual impedances to improve the power sharing in a droop controlled, islanded microgrids. The difference between implementing the virtual impedance in the stationary and the synchronous reference frames has been discussed. Moreover, the difference in how to account for the transient term of the virtual impedance has been shown, and a comparison between the quasi-stationary approach and the low-pass filtered derivative term has been carried out. In particular, the effect of including the transient term of the virtual impedance is highlighted by constructing a state-space small-signal model. Both the modal analysis on the small-signal model and the results of the numerical simulations

This is the accepted version of an article published in 2018 IEEE International Conference on Environment and Electrical Engineering and 2018 IEEE Industrial and Commercial Power Systems Europe - EEEIC/I&CPS Europe
DOI: 10.1109/EEEIC.2018.8493932

indicate that the damping of the system is improved by including the transient term.

ACKNOWLEDGMENT

This project has received funding through the research centre for environmentally friendly energy CINELDI (Centre for Intelligent Electricity Distribution), supported by the Research Council of Norway.

REFERENCES

[1] R. H. Lasseter. MicroGrids. *2002 IEEE Power Engineering Society Winter Meeting. Conference Proceedings (Cat. No.02CH37309)*, 1:305–308, 2002.

[2] J. Rocabert, A. Luna, F. Blaabjerg, and P. Rodríguez. Control of Power Converters in AC Microgrids. *IEEE Transactions on Power Electronics*, 27(11):4734–4749, 2012.

[3] D. E. Olivares, A. Mehrizi-Sani, A. H. Etemadi, C. A. Cañizares, R. Iravani, M. Kazerani, Amir H. Hajimiragha, Oriol Gomis-Bellmunt, Maryam Saeedifard, Rodrigo Palma-Behnke, Guillermo A. Jiménez-Estévez, and Nikos D. Hatziargyriou. Trends in microgrid control. *IEEE Transactions on Smart Grid*, 5(4):1905–1919, 2014.

[4] Y. Mohamed and E. F. El-Saadany. Adaptive Decentralized Droop Controller to Preserve Power Sharing Stability of Paralleled Inverters in Distributed Generation Microgrids. *IEEE Transactions on Power Electronics*, 23(6):2806–2816, 2008.

[5] J. M. Guerrero, L. G. Vicuña, J. Matas, M. Castilla, and J. Miret. Output impedance design of parallel-connected UPS inverters with wireless load sharing control. *IEEE Transactions on Industrial Electronics*, 52(4):1126–1135, 2005.

[6] Y. W. Li and C. Kao. An accurate power control strategy for power-electronics-interfaced distributed generation units operating in a low-voltage multibus microgrid. *IEEE Transactions on Power Electronics*, 24(12):2977–2988, 2009.

[7] X. Wang, Y. W. Li, F. Blaabjerg, and P. C. Loh. Virtual-Impedance-Based Control for Voltage-Source and Current-Source Converters. *IEEE Transactions on Power Electronics*, 30(12):7019–7037, 2015.

[8] J. M. Guerrero, J. Matas, L. G. Vicuña, M. Castilla, and J. Miret. Decentralized control for parallel operation of distributed generation inverters using resistive output impedance. *IEEE Transactions on Industrial Electronics*, 54(2):994–1004, 2007.

[9] J. He and Y. W. Li. Analysis, Design, and Implementation of Virtual Impedance for Power Electronics Interfaced Distributed Generation. *IEEE Transactions on Industry Applications*, 47(6):2525–2538, 11 2011.

[10] P. Zhang, H. Zhao, H. Cai, J. Shi, and X. He. Power decoupling strategy based on virtual negative resistor for inverters in low-voltage microgrids. *IET Power Electronics*, 9(5):1037–1044, 2016.

[11] N. Pogaku, M. Prodanović, and T. C. Green. Modeling, analysis and testing of autonomous operation of an inverter-based microgrid. *IEEE Transactions on Power Electronics*, 22(2):613–625, 2007.

[12] Y. Tao, Q. Liu, Y. Deng, X. Liu, and X. He. Analysis and mitigation of inverter output impedance impacts for distributed energy resource interface. *IEEE Transactions on Power Electronics*, 30(7):3563–3576, 2015.